This manuscript is now published at: https://doi.org/10.1029/2023JB026706

This manuscript is now published in Journal of Geophysical Research: Solid Earth and is available fully open access. Please cite the published version: https://doi.org/10.1029/2023JB026706

This manuscript is now published at: https://doi.org/10.1029/2023JB026706

Rapid fault healing after seismic slip

John D. Bedford[1,2*], Takehiro Hirose[1] and Yohei Hamada[1]

[1]Kochi Institute for Core Sample Research (X-star), Japan Agency for Marine-Earth Science and Technology (JAMSTEC), 200 Monobe-otsu, Nankoku, Kochi 783-8502, Japan

[2]Now at Department of Earth, Ocean and Ecological Sciences, University of Liverpool, Liverpool, L69 3GP, UK

*Corresponding author: John Bedford (jbedford@liverpool.ac.uk)

Key Points

- We investigate fault healing behavior of gabbro and granite gouges after they have experienced dynamic weakening during high-velocity slip
- Once slip has ceased, the fault gouges rapidly recover the strength they lost during the high-velocity slip events
- Enhanced healing is likely caused by thermally activated chemical bonding at asperity contacts in the gouge

This manuscript is now published at: https://doi.org/10.1029/2023JB026706

Abstract

Fault strength recovery (healing) following an earthquake is a key process in controlling the recurrence of future events; however, the rates and mechanisms of fault healing are poorly constrained. Here, by performing high-velocity friction experiments at seismic slip rates (0.57 m/s), we show that granite and gabbro fault gouges recover their strength rapidly after experiencing dynamic weakening. The healing rates are one to two orders of magnitude faster than those observed in typical frictional healing experiments performed at slow slip velocities (micrometers to millimeters per second). Analysis of the sheared gouges using Raman spectroscopy suggests that enhanced healing after seismic slip is associated with thermally activated chemical bonding at frictional contacts in the gouge. Our results indicate that seismogenic faults can potentially regain their strength early during interseismic periods, which would imply that healing may not be the dominant control on earthquake recurrence, with other processes, such as far-field tectonic loading or frictional stability transitions, possibly dictating the occurrence of future events.

Plain Language Summary

During an earthquake, faults experience a dynamic reduction in their frictional strength due to processes such as shear heating. How quickly faults can regain their strength (i.e., heal) after an earthquake is important for controlling when future events might occur. Here, we perform high-velocity shearing experiments on simulated faults – at similar slip speeds that natural faults slide at during real earthquakes - to investigate how faults weaken and then subsequently recover their strength during and after a seismic event. We find that our experimental faults recover their strength rapidly after a seismic slip event, with the rate of strength recovery being one to two orders of magnitude faster than healing rates typically observed in traditional frictional healing experiments performed at much slower sliding velocities. We perform chemical analyses on our sheared faults and find a change in the chemical bonding properties of the fault surface after a simulated earthquake event. We therefore hypothesize that the rapid fault restrengthening we observe once the fault has stopped slipping is caused by enhanced chemical bonding at frictional

This manuscript is now published at: https://doi.org/10.1029/2023JB026706

contacts along the experimental faults. Our results suggest that natural tectonic faults will recover their strength quickly after an earthquake has occurred.

1. Introduction

Faults slip suddenly during earthquakes, accelerating to velocities on the order of a few meters per second. At these seismic slip velocities, a significant reduction in fault strength occurs (Di Toro et al., 2011) as a result of various dynamic weakening mechanisms becoming activated by shear heating and/or grain size reductions (Tullis, 2015). Although our knowledge of dynamic fault weakening processes has increased significantly over the last 25 years since the advent of high-velocity friction experiments (Tsutsumi & Shimamoto, 1997), our understanding of how faults regain their strength after dynamic weakening, once seismic slip has ceased, is more limited. Fault restrengthening is a fundamental process in the earthquake cycle that may control the recurrence time (Vidale et al., 1994), the mode of slip (Shreedharan et al., 2023), the maximum strength that can be attained (Kanamori & Allen, 1986; Scholz et al., 1986), and the nature of radiated energy (McLaskey et al., 2012) in future events.

The rate of fault restrengthening can vary with both time and space along a fault during the earthquake cycle (Li et al., 2006; Pei et al., 2019). Restrengthening may occur initially during coseismic slip itself, as sometimes observed during the deceleration phase of high-velocity friction experiments (e.g., Harbord et al., 2021; Proctor et al., 2014; Sone & Shimamoto, 2009; Violay et al., 2019). Coseismic restrengthening (Fig. 1) is a potentially important process in the generation of pulse-like earthquake ruptures (Galetzka et al., 2015; Heaton, 1990), which require that the just-slipped portions of a fault rapidly regain their strength (self-heal) shortly after the passage of the rupture front in order to prevent further slip; in contrast to crack-like ruptures where slip continues behind the rupture front for the duration of the rupture event. However, the mechanisms of coseismic restrengthening are poorly constrained and it is a phenomenon that is not always observed in experiments, or it may only partially recover the strength lost during high-velocity fault slip (e.g., Boulton et al., 2017; Han et al., 2007; Hunfeld et al., 2021; Seyler et al., 2020; Yao et al., 2013).

In such cases, the majority of fault restrengthening must occur in the postseismic regime instead, when the fault is held in quasi-stationary contact.

The process of strength recovery as a fault is held in quasi-stationary contact, known as fault healing, has been extensively studied in experiments performed at slow sliding velocities, on the order of micrometers per second (e.g., Beeler et al., 1994; Carpenter et al., 2016; Dieterich, 1972; Marone, 1998; Marone & Saffer, 2015). The common procedure for studying fault healing in the laboratory is to perform slide-hold-slide (SHS) experiments (Dieterich, 1972; Marone, 1997), whereby the shearing of fault materials is paused for predetermined durations and then shear strength is monitored as sliding is resumed after the hold period. Previous low-velocity SHS experiments have shown that frictional strength typically increases linearly with the logarithm of hold time (Baumberger & Caroli, 2006; Beeler et al., 1994; Carpenter et al., 2016; Dieterich, 1972; Marone & Saffer, 2015), with healing rate being dependent on the composition of the fault materials (Carpenter et al., 2016); although it should be noted that some materials (e.g., clays) have been reported to display a negative or near-zero change in frictional strength with hold time (e.g., Orellana et al., 2018; Shreedharan et al., 2023). The physical mechanisms responsible for fault healing are debated, with time-dependent growth of real contact area due to asperity creep often invoked to explain healing behavior (Dieterich & Kilgore, 1994). However, more recent work has suggested other processes such as chemical bond formation could be responsible for fault healing observed in laboratory experiments (Li et al., 2011; Thom et al., 2018).

This manuscript is now published at: https://doi.org/10.1029/2023JB026706

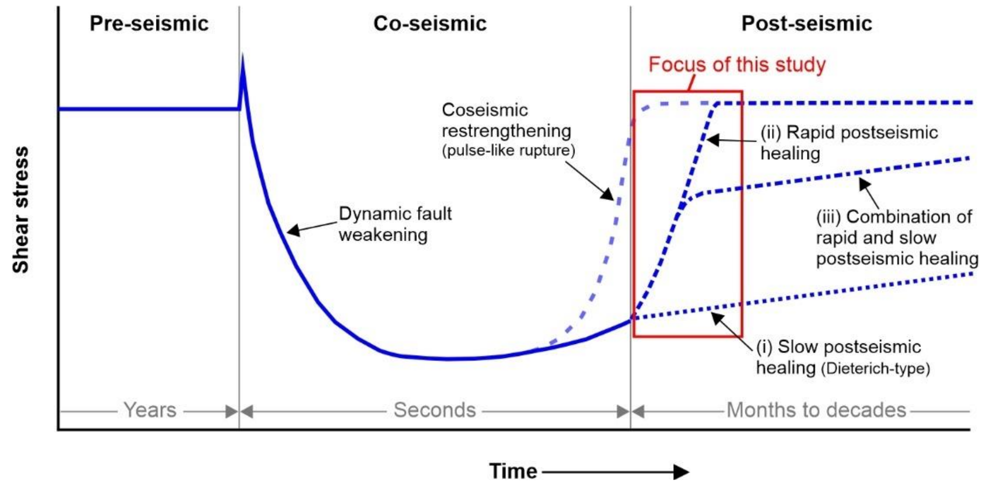

Figure 1: *Schematic diagram of fault strength evolution during the seismic cycle. During coseismic slip, a significant reduction in shear stress occurs as a result of dynamic fault weakening. In the postseismic regime the fault regains its strength as it is held in quasi-stationary contact. The aim of this study is to determine whether fault strength recovery immediately following seismic slip occurs via (i) slow "Dieterich-type" healing, (ii) rapid postseismic healing, or (iii) a combination of rapid and slow healing.*

In some specific cases, the healing rates determined from low-velocity SHS experiments correlate well with stress drops observed during sequences of small repeating earthquakes in nature (i.e., the magnitude of the stress drop increases as the duration of the recurrence interval increases (Marone et al., 1995; Vidale et al., 1994)). However, following large earthquakes, geophysical observations suggest that rapid fault restrengthening can occur in comparison to typical recurrence intervals, with the majority of the strength being recovered early during the interseismic period. For example, shear-wave splitting measurements following the 1995 Kobe earthquake (moment magnitude M_w 6.9) on the Nojima fault indicate that the majority of fault strength had recovered within 33 months of the main event (recurrence interval of approximately 2000 years) (Tadokoro & Ando, 2002). Borehole permeability measurements from the Longmenshan fault zone that hosted the 2008 Wenchuan earthquake (M_w 7.9), suggest that the fault healed within 0.6 to 2.5 years after the earthquake (Xue et al., 2013). Seismic velocity measurements made following the same event, and also the nearby 2013 Lushan earthquake (M_w 6.6), support the notion of rapid healing on the fault (Pei et al., 2019), with similar enhanced strength recovery rates also inferred after the 2004 Parkfield earthquake (M_w 6.0) on the San Andreas fault (Li et al., 2006) and between the 2019 Ridgecrest earthquake pair (M_w 6.4 and M_w 7.1) in the eastern California shear zone (Magen et al., 2020). Geophysical observations thus potentially indicate that different postseismic healing processes are in operation immediately following large earthquakes, leading to more rapid restrengthening, than the classic "Dieterich-type" healing mechanisms (Dieterich, 1972; Dieterich & Kilgore, 1994) responsible for fault strengthening in low-velocity SHS experiments (Fig. 1). It should also be noted that over typical recurrence intervals of large earthquakes (up to several hundreds of years), processes such as cementation and pressure solution will increase cohesion of fault materials, contributing to the long-term strength evolution of the fault during interseismic periods (van den Ende & Niemeijer, 2019; Muhuri et al., 2003; Tenthorey & Cox, 2006).

In order to investigate rapid postseismic healing processes in the laboratory we need to simulate earthquake slip velocities, something that is not done in typical low-velocity SHS experiments. By shearing at seismic slip velocities, the fault materials will also experience dynamic weakening (Di Toro et al., 2011), which more closely mimics what happens during natural earthquakes. Here, we perform high-velocity (0.57 m/s) SHS experiments on gabbro and granite gouges under room humidity conditions at a constant normal stress of 1.5 MPa in all experiments, to investigate how the gouges regain their strength during quasi-stationary hold periods after experiencing dynamic weakening. We varied the duration of the static hold period in order to determine whether the postseismic restrengthening behavior exhibits either, (i) "Dieterich-type" healing as observed in low-velocity SHS experiments, (ii) a form of more rapid healing, or (iii) a combination of rapid and slow healing; as shown schematically in Figure 1. We then analyze the microstructures of the sheared gouges and perform Raman spectroscopy in an attempt to elucidate the underlying healing mechanisms in operation after seismic slip events.

This manuscript is now published at: https://doi.org/10.1029/2023JB026706

2. Methods

2.1. Experimental procedure

The experimental samples were produced by crushing and sieving intact samples of Inada granite and Belfast gabbro to form simulated fault gouges (powders) with grain sizes between 63-125 μm. A layer of simulated gouge (measured by weight to produce a layer with an initial thickness of 1.5 mm) was then sandwiched between two cylindrical stainless steel experimental forcing blocks (diameter = 25 mm). The surface of the blocks contains radial grooves (0.5 mm deep) to minimize boundary shear between the gouge layer and the forcing blocks during the experiments. To limit gouge loss during shearing, the gouge layer was contained laterally by a 5 mm thick polytetrafluoroethylene (PTFE) sleeve (Fig. 2b). The low-friction PTFE sleeve was cut and tightened onto the forcing blocks using a hose clip (Fig. 2c-d), following the procedure outlined in the supplementary material of De Paola et al., (2015). We used a torque-screwdriver to ensure the hose clip was tightened by the same amount for each experiment. Once the gouge sample was constructed in between the forcing blocks, it was sheared using the PHV rotary shear apparatus (Fig. 2a) in the Rock Mechanics Laboratory at the Kochi Institute for Core Sample Research (Japan).

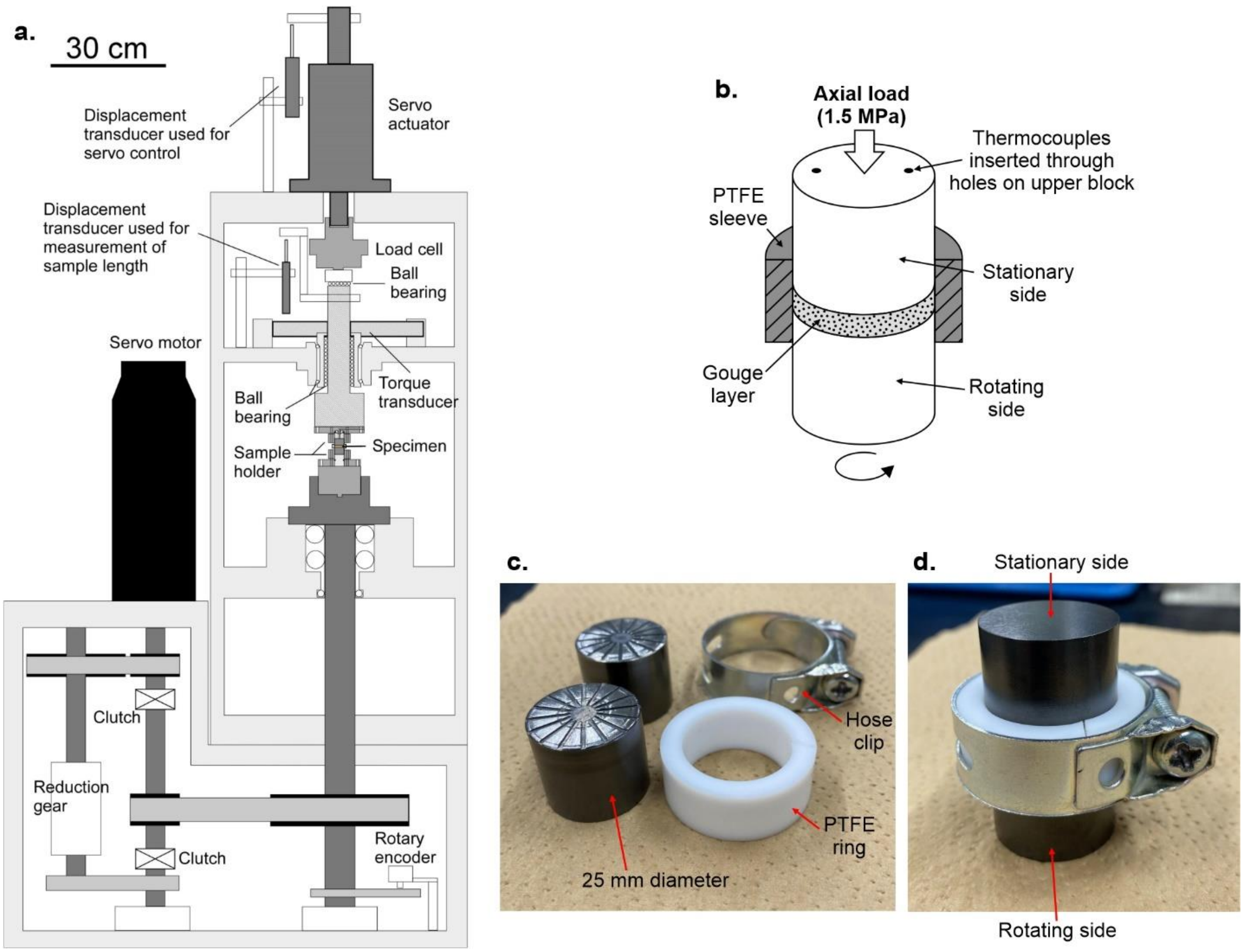

__Figure 2. (a)__ Schematic diagram of the PHV rotary shear apparatus (modified from Tanikawa et al., (2012)). __(b)__ Schematic diagram of the experimental sample configuration. The gouge layer is sandwiched between two cylindrical steel experimental forcing blocks and contained laterally by a PTFE ring. __(c)__ Photograph of the disassembled components of the sample assembly. __(d)__ Photograph of the assembled sample setup; the PTFE ring is cut and then tightened on to the assembly using a hose clip.

Before the main SHS experiment, the gouge samples were pre-sheared for four complete revolutions (equivalent to 0.2 m of slip, measured at 2/3 the radius of the cylindrical specimens) under a normal stress of 0.75 MPa at a rate of 1.7 mm/s, to ensure the gouge layer thickness was even across the sample. The normal stress was then increased to the experimental target value of 1.5 MPa. As all experiments were run under the same normal stress we did not correct for the shear stress contribution from the PTFE sleeve, with previous work showing that the mechanical contribution from the PTFE is negligible (Seyler et al., 2020). All tests were conducted under room temperature (22-25 °C) and humidity (30-50%) conditions. We chose to run the experiments without a pore fluid to avoid any transient fluid pressure effects caused by processes such as thermal pressurization (e.g., Badt et al., 2020; Rice, 2006), which could affect the frictional strength evolution as they dissipate during the hold period. As the slip velocity varies with radial position, we use an "equivalent slip velocity" (v_e) which corresponds to the velocity at 2/3 of the radius of the cylindrical specimens (De Paola et al., 2015), given by:

$$v_e = \frac{4\pi Rr}{3}$$

where R is the revolution rate of the motor and r is the sample radius. In our experiments, the gouge layers were sheared at 0.57 m/s for an equivalent slip displacement (d_e) of 15 m (650 rpm for 285 revolutions) during the first sliding event (slide 1, in Fig. 3), they were then held in quasi-stationary contact for a predetermined amount of time (hold times ranging from 1.7 to 7200 s), before being sheared again for another 15 m at 0.57 m/s (slide 2).

In some of the high-velocity experiments temperature measurements were made by placing thermocouples next to the upper surface of the gouge layer (<0.5 mm above the gouge surface). Two holes were drilled into the upper experimental forcing block (on the stationary side of the fault, Fig. 2b) and thermocouples were inserted and sealed into place using a ceramic bond. The thermocouples were positioned at 2/3 of the radius so that the temperature measurements were consistent with the calculated v_e and d_e.

As well as the high-velocity SHS experiments, some additional tests were performed at micrometer-per-second slip velocities to compare healing rates after low-velocity slip with the rates determined in our high-velocity experiments. In the low-velocity SHS experiments (performed at an equivalent slip velocity of 2.6 μm/s) we used intact cylindrical rock-to-rock samples of Inada granite and Belfast gabbro, instead of gouge. Initially we tried performing the low-velocity SHS experiments using gouge samples, however, we found negligible healing even after hold periods >1000 s (healing rate, $\beta \approx 0$), with steady-state strength being achieved in <50 μm of slip upon reshearing after the hold. We believe this is due to the low normal stress conditions and also low shear strain the gouge had experienced before the low-velocity SHS experiments were performed. We tried to perform experiments where the gouges were sheared at millimeter-per-second slip velocities to an equivalent slip displacement of 15 m prior to the low-velocity SHS tests (i.e., the same d_e as achieved in the high-velocity SHS experiments), however, there was a large amount of gouge extrusion from between the PTFE ring and the metal forcing blocks during the pre-shearing. Therefore, as the purpose of our low-velocity SHS experiments is just to provide an approximate representation of typical healing rates at slow sliding velocities, we chose to instead include data from rock-to-rock samples in Fig. 4, as the healing rates we determined from the rock-to-rock samples are close to previously reported healing rates observed in many low-velocity friction studies on both gouge and intact rock samples of granite and gabbro (e.g., Beeler et al., 1994; Carpenter et al., 2016; Giacomel et al., 2021; Mitchell et al., 2013). Prior to the low-velocity SHS experiments, the cylindrical rock samples were rotated for more than 1000 rotations at a constant speed of 4 rpm ($v_e = 3.5$ mm/s) over a range of incrementally increasing normal stresses from 0.3 to 1.4 MPa. The purpose of this procedure was to remove any heterogeneities and ensure the surfaces on opposites side of the sliding interface were parallel. The wear materials produced on the sliding surface during this pre-sliding were not removed before the SHS experiments, thus the rock samples were separated by a thin gouge layer (~50 μm thickness) during the experiments (Fig. S1). The wear materials produced during the experiments were allowed to extrude from the slip zone (we did not use a PTFE containing ring for these tests). Once the sliding surface was prepared, the normal stress was increased to 1.5 MPa and the samples were sheared for 0.26 mm during each sliding event in the SHS experiment at a velocity of 2.6 μm/s; the length of the hold time between the sliding events was varied to determine the healing rate (hold times ranging from 7 to 7340 s).

2.2. Raman spectroscopy

After the experiments the PTFE ring was removed and the sample holders were gently opened to expose the sheared gouge sample. The surface of the gouge was then analyzed using Raman spectroscopy. (Note that Raman spectra were acquired on the exposed gouge surface before it was impregnated with epoxy resin and prepared for microstructural imaging). Raman spectra of the test samples were obtained with a 514.5 nm Ar laser (Showa Optronics Co., Ltd.) and T64000 Raman system (Jobin Yvon Horiba). The laser passed through a 40× objective and the laser power at the sample surface was set at 2–5 mW. The scattered light was collected by backscattered geometry with a 25 μm pinhole and a holographic notch filter, and finally dispersed using a 1800 grids/mm grating and analyzed by a Peltier cooled CCD detector (SPECTRUM ONE, Jobin Yvon Horiba). Spatial resolution is about 1 μm, and wavenumber resolution is about 1 cm^{-1}. Frequencies of the Raman bands were calibrated by measuring silicon standards.

3. Results

3.1. Friction data

The frictional strength evolution of the granite and gabbro gouge samples is shown in Figure 3 for both sliding events in the SHS experiments. During the first high-velocity sliding event (slide 1) the gouge layers experience dynamic weakening with the friction coefficient (μ) decreasing by ~0.25, from a peak value between 0.7-0.8, to a final value of ~0.5 after 15 m of slip (Fig. 3a and c). This amount of weakening is comparable to previous experimental studies performed under similar normal stress and velocity conditions (e.g., Seyler et al., 2020), with greater weakening (to $\mu \approx 0.2$) typically observed when gouges are sheared under higher normal stresses (Pozzi et al., 2021; Seyler et al., 2020) or at faster sliding velocities (Boulton et al., 2017; Yao et al., 2013) than in our experiments. During the static hold period between sliding events in our experiments the gouge undergoes healing, with the peak friction of the second sliding event (slide 2) being dependent on the duration of the hold period (Fig. 3b and d) – i.e., longer hold periods lead to higher peak friction values. During slide 2, after reaching their respective peak friction values, the gouge layers again experience dynamic weakening, returning to a final μ of ~0.5 after another 15 m of high-velocity slip.

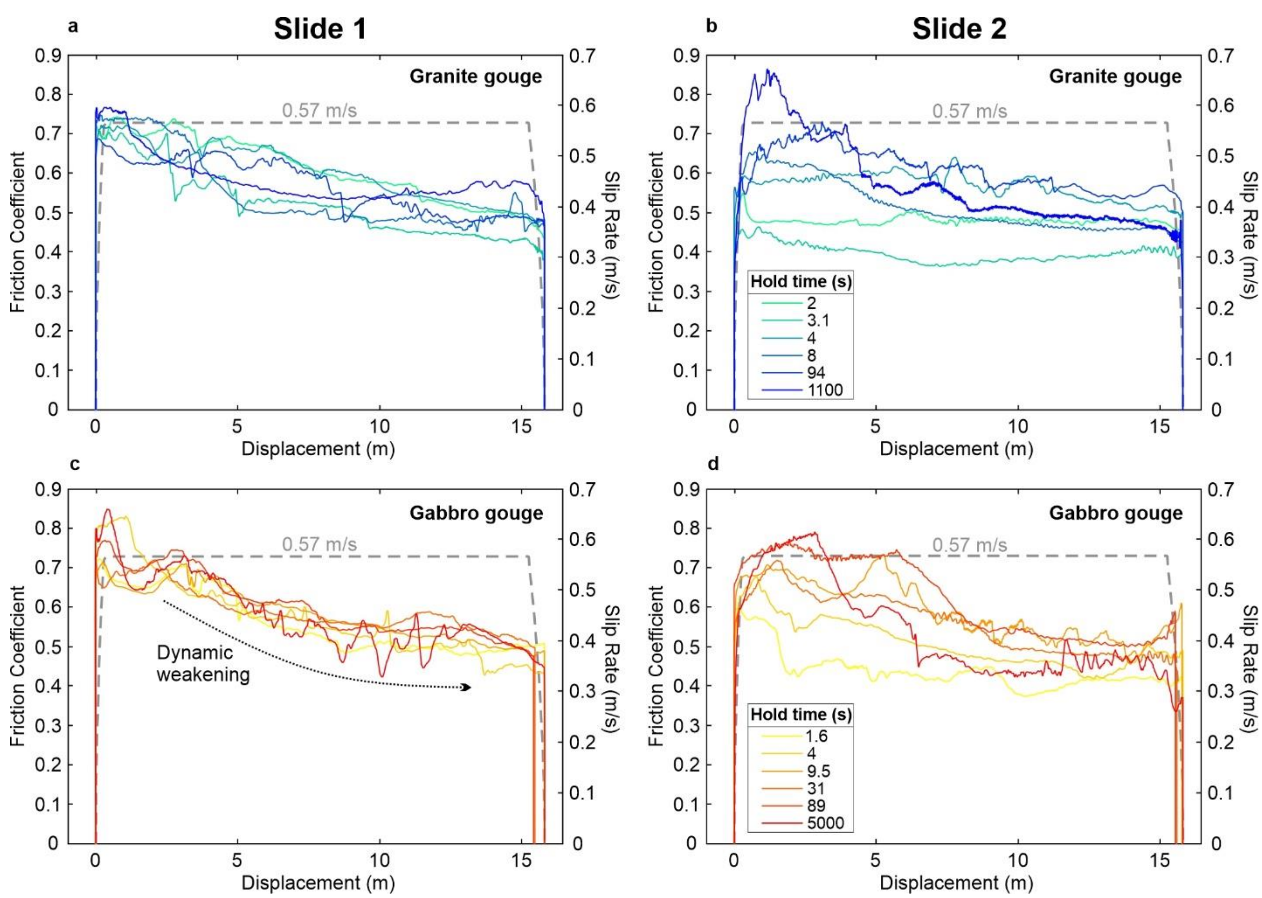

Figure 3: *Example mechanical data from the two high-velocity sliding events in the slide-hold-slide experiments. The plots show the evolution of the friction coefficient with displacement for the granite gouge during (**a**) the first sliding event (slide 1), and (**b**) the second sliding event (slide 2). The same data are shown for the gabbro gouge in panels (**c**) and (**d**), respectively. The velocity-displacement history during the experiments is shown by the grey dashed line. The gouge layers all show similar dynamic weakening during slide 1, with the friction coefficient decreasing by ~0.25 after 15 m of displacement. The peak friction*

during slide 2 is controlled by the duration of the static hold time between the sliding events, with longer hold times leading to higher peak friction.

The gouge samples recover their strength rapidly during the static hold period, as shown in Figure 4 where $\Delta\mu$ (the difference between the peak friction of slide 2 (μ_{p2}) and the final friction of slide 1 (μ_{f1}), $\Delta\mu = \mu_{p2} - \mu_{f1}$; see also Fig. S2) is plotted against hold time. After around 20 s of static hold, the granite gouge had recovered the majority of the strength it lost during slide 1, with the gabbro gouge healing even more rapidly (<10 s of static hold). For comparison, healing data from low-velocity SHS experiments performed on intact samples of granite and gabbro at slip rates of 2.6 μm/s has been included in Figure 4 (see Methods for more details). The healing rate ($\beta = \Delta\mu/\Delta\log{(t_h)}$, where t_h is the hold time) is around two orders of magnitude greater for the experiments performed at seismic slip velocities than those performed at micrometer per second slip velocities (Fig. 4). After the initial rapid strength recovery in the high-velocity tests (β > 0.1), the healing rate decreased to a rate that is comparable to those observed in the low-velocity SHS experiments (β < 0.01), which is largely consistent with healing rates reported in previous low-velocity friction studies on granitic and basaltic fault materials (Beeler et al., 1994; Carpenter et al., 2016; Giacomel et al., 2021; Mitchell et al., 2013); see Table 1 for compilation of healing rates reported in previous studies.

A major difference between high-velocity and low-velocity SHS experiments is that during high-velocity slip there is a large temperature increase caused by shear heating, which is much less significant during sliding at low-velocity. In order to measure the temperature evolution in our high-velocity SHS experiments, we placed thermocouples next to the upper surface of the gouge layer on the stationary side of the fault in some experiments (see Methods). We recorded peak temperatures of around 350-400 °C during the high-velocity sliding events, with the temperature decaying as the samples cooled during the hold period, returning to the ambient temperature in the laboratory after several minutes of static hold (Fig.

4). However, we find that the rapid frictional healing, which begins immediately after the initiation of the hold period, occurred when the gouge layer was still relatively hot, at temperatures >200 °C (Fig. 4).

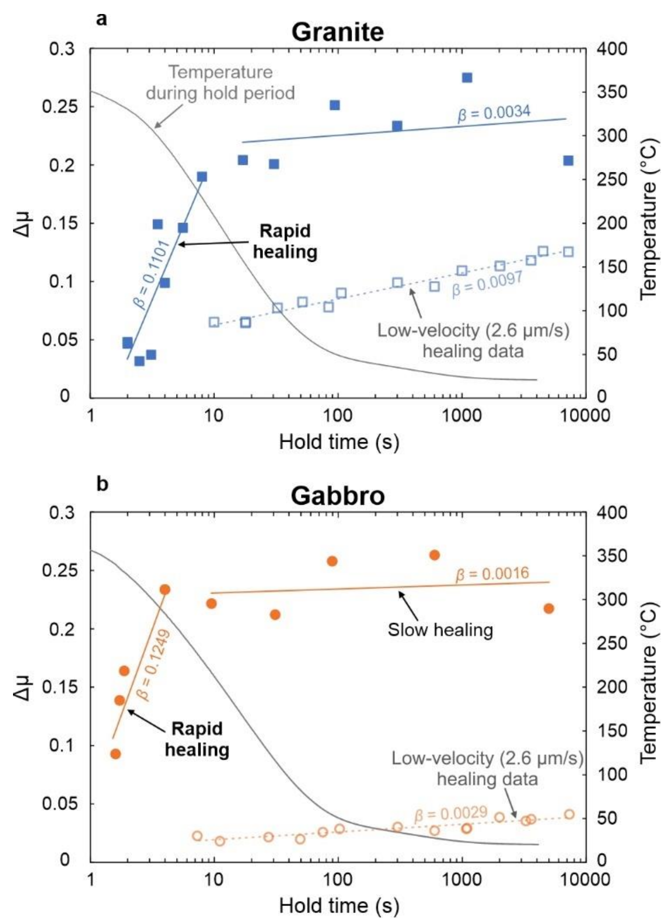

Figure 4: *Frictional healing data from the high-velocity SHS experiments. The slide-hold-slide parameter* $\Delta\mu$ *is plotted against hold time for (**a**) granite gouge and (**b**) gabbro gouge. The gouges experience rapid healing immediately after the initiation of the hold period; the healing rate then decreases to a rate comparable to those observed in low-velocity SHS experiments. Healing data from experiments performed at 2.6 μm/s has been included (hollow symbols) for comparison. The temperature evolution was monitored during the hold period (grey line); rapid healing occurs while the gouges are still relatively hot (>200 °C) after the high-velocity first sliding event.*

Material	**Study**	**Sample type**	**β**	**Sliding Vel. (m/s)**	**σ'_n (MPa)**	**Atmospheric conditions**
High-velocity SHS experiments:						
Granite	This study	Gouge	0.1101	0.57	1.5	Room dry
Gabbro	This study	Gouge	0.1244	0.57	1.5	Room dry
Pingxi fault gouge	[1]	Gouge	0.154-0.188	1.4	0.8	Room dry
Intermediate-velocity SHS experiments:						
Granite	[2]	Bare rock*	0.18	0.085	0.62	Room dry or water saturated
Gabbro	[2]	Bare rock*	0.29	0.085	0.62	Room dry or water saturated
Low-velocity SHS experiments (granitic/gabbroic materials):						
Granite	This study	Bare rock	0.0097	2.6×10^{-6}	1.5	Room dry
Gabbro	This study	Bare rock	0.0029	2.6×10^{-6}	1.5	Room dry
Granite	[3]	Gouge	0.007	1×10^{-5}	20	100% relative humidity
Granite	[4]	Bare rock	0.014	1×10^{-6}	25	Room dry
Granite	[5]	Bare rock	0.016 to 0.021	1×10^{-5}	15	Room dry, T = 20-550 °C
Granite	[6]	Bare rock	0.009	1×10^{-7}	20	Water saturated, P_f = 10 MPa
Basalt	[7]	Gouge	0.0051 to 0.0063	1×10^{-5}	5-30	Room dry
Basalt	[7]	Gouge	0.0091 to 0.0128	1×10^{-5}	5-30	Water saturated
Basalt	[7]	Bare rock	0.0211 to 0.0265	1×10^{-5}	5-30	Room dry or water saturated
Low-velocity SHS experiments (other materials):						
Quartz	[8]	Gouge	0.007 to 0.012	0.5 to 100×10^{-6}	25	Room dry
Quartz	[9]	Gouge	0.0082 to0.0086	1 to 10×10^{-6}	25	Room dry
Quartz	[3]	Gouge	0.006	1×10^{-5}	20	100% relative humidity
Andesine feldspar	[3]	Gouge	0.007	1×10^{-5}	20	100% relative humidity
Biotite	[3]	Gouge	0.001	1×10^{-5}	20	100% relative humidity
Ca montmorillonite	[3]	Gouge	0.002	1×10^{-5}	20	100% relative humidity
Kaolinite	[3]	Gouge	0.003	1×10^{-5}	20	100% relative humidity
Talc	[3]	Gouge	0.0005	1×10^{-5}	20	100% relative humidity
Scaly clays	[10]	Gouge	-0.0362 to 0.015	1×10^{-5}	4-20	Water saturated
Hikurangi sediments	[11]	Gouge	<0.0001	1 to 30×10^{-6}	25	Water saturated, P_f = 5-10 MPa
Serpentinite	[12]	Gouge	-0.003 to 0.010	1×10^{-5}	2-40	Water saturated, P_f = 1.5-10 MPa
Carrara marble	[13]	Bare rock	0.0046	1×10^{-6}	1	Room dry or N_2 atmosphere
Fault mirror surface	[13]	Bare rock	0.00093	1×10^{-6}	1	Room dry or N_2 atmosphere
Halite	[14]	Gouge	Non-log-linear	1×10^{-5}	1-5	Water saturated
Hydrothermal SHS experiments:						
Quartz	[15]	Gouge	0.010 to 0.014	1×10^{-5}	50	P_f = 10 MPa, T = 25-200 °C
Granite	[6]	Bare rock	-0.044 to 0.013	1×10^{-7}	20	P_f = 10 MPa, T = 200 °C

Table 1: *Collation of healing rates (β) reported in previous SHS experimental studies, along with the sliding velocity, effective normal stress (σ'_n) and atmospheric conditions in each study. The reference studies listed are:* ***[1]*** *Yao et al., (2013);* ***[2]*** **Mizoguchi et al., (2009);* ***[3]*** *Carpenter et al., (2016);*

[4]** Beeler et al., (1994); **[5]** Mitchell et al., (2013); **[6]** Jeppson and Lockner (2022); **[7]** Giacomel et al., (2021); **[8]** Marone (1997); **[9]** Marone (1998); **[10]** Orellana et al., (2018); **[11]** Shreedharan et al., (2023); **[12] Scuderi & Carpenter (2022)*; **[13]*** Park et al., (2021)*; **[14]** van den Ende and Niemeijer (2019); **[15]** Nakatani and Scholz (2004). *Note that in the intermediate velocity SHS experiments of Mizoguchi et al., (2009) there is a thin gouge layer (approx. 50 μm thickness) present between the intact rock samples, formed as a result of frictional wear of the bare rock surfaces during pre-sliding before the SHS experiments. Also note that in the hydrothermal SHS experiments there is typically a complex healing relationship with hold time, with β varying over long hold durations.*

During the static hold period the normal stress is well distributed across the gouge layer and maintained at a constant value of 1.5 MPa (Fig. 5a and b). There is, however, some compaction of the gouge during the hold period (Fig. 5c and d), as measured by the displacement transducer attached to the axial piston of the rotary shear apparatus (Fig. 2a). The shortening of the gouge layer as a result of compaction is non-linear when plotted against the logarithm of hold time (Fig. 5e and f), particularly during the initial stages of the hold period (<20 s) where rapid healing of the frictional strength occurs (Fig. 4). Compaction/dilation data for the gouge layers during the high-velocity sliding events in the SHS experiments is presented in Figure S3.

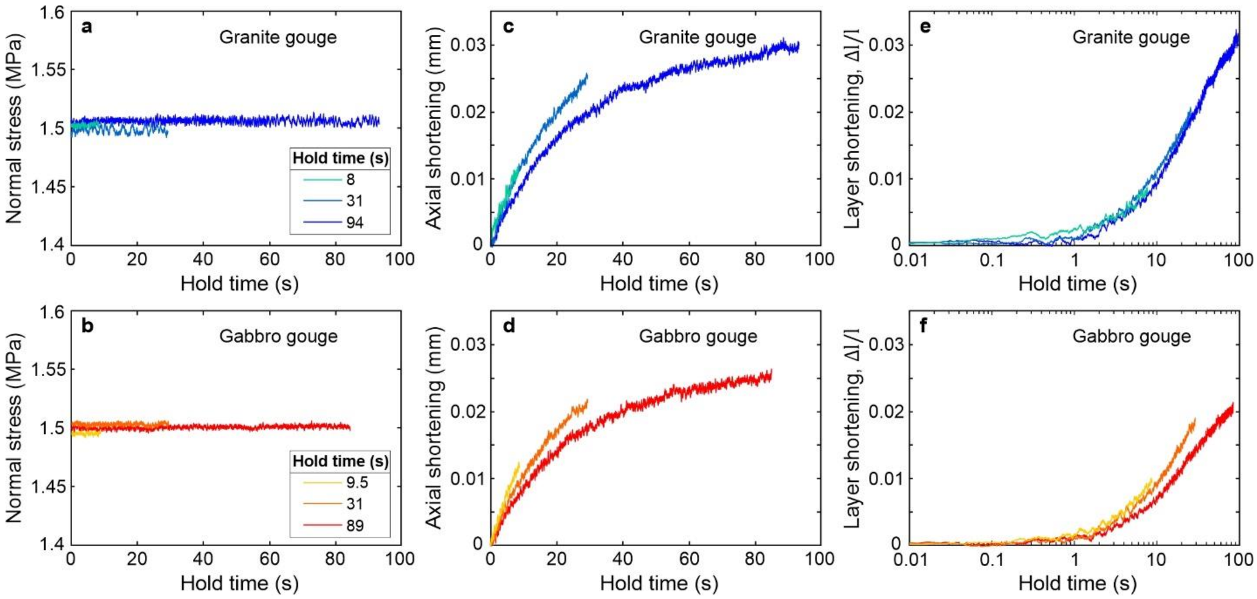

Figure 5: *Examples of normal stress* ***(a, b)*** *and axial shortening* ***(c, d)*** *data during the static hold periods in the high-velocity SHS experiments for both the granite and gabbro gouges. Panels* ***(e)*** *and* ***(f)*** *show gouge layer shortening ($\Delta l/l$, where l is the layer thickness) against hold time for the granite and gabbro gouges, respectively, where hold time is plotted on a logarithmic scale. Note that for experiments where the hold time >100 s, data logging was paused during the hold period to reduce the file size, therefore we do not have continuous normal stress and axial displacement data for hold durations >100 s.*

3.2. Microstructural analysis and Raman spectroscopy

We analyzed the microstructures of the sheared gouges by collecting backscatter electron (BSE) and secondary electron (SE) images using a JEOL JSM-6500F field emission scanning electron microscope (FE-SEM). Fig. 6a-b shows BSE images of granite and gabbro gouge samples after the SHS experiments, where the sheared layers have been cut perpendicular to the shear plane and parallel to the shearing direction at a distance equal to 2/3 of the sample radius. (Note that the gouge layers were vacuum impregnated with a low-viscosity epoxy resin before being cut and polished ready for BSE imaging). The sheared gouges display a texture of well-rounded larger relict grains surrounded by fine-grained highly comminuted material, indicating that they have undergone a significant grain size reduction and particle roundening when compared to the starting gouge material (see Fig. S4), with this likely occurring via mechanical grinding (Sammis & Ben-Zion, 2008). In the granite gouge the deformation appears to be homogeneously distributed across the layer (Fig. 6b), whereas the gabbro gouge displays evidence of a highly comminuted localized zone at the boundary of the layer (Fig. 6a and c). Despite the apparent difference in localization behavior between the different materials, their mechanical behavior is remarkably similar (Fig. 3), suggesting that shear localization does not have a strong control on frictional strength evolution under these experimental conditions. Our experiments were run under relatively low normal stress, previous studies suggest that localization would become more prominent if the gouge layers were sheared under higher normal stress (Bedford & Faulkner, 2021; Rempe et al., 2020), or if they were taken to greater shear strains (Kaneki et al., 2020).

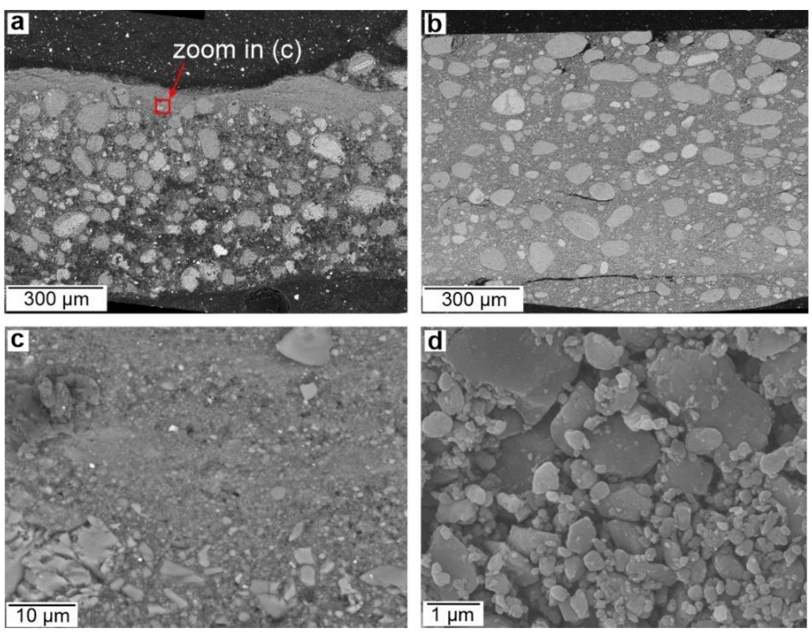

Figure 6: *Backscatter electron images of (**a**) gabbro and (**b**) granite gouge layers recovered at the end of the SHS experiments after both sliding events (total displacement = 30m, which equates to a bulk shear strain (γ) of approximately 20,000). (**c**) Zoom of the localized zone within the gabbro gouge layer (from*

the red box in (a)). ***(d)*** *Secondary electron image of the surface of the gabbro gouge layer showing the presence of sub-micron particles.*

The rapid healing observed after sliding at seismic slip rates in our experiments (Fig. 4) must be caused by a strengthening of the frictional contacts in the gouge layer, possibly as a result of enhanced interfacial chemical bonding. To investigate further the possible causes of the rapid restrengthening, we analyzed the sheared gouges using Raman spectroscopy, as this provides information about the chemical structure of the gouge surface. We found that the gouges sheared at high-velocity all showed the appearance of a small broad peak in the Raman spectra at a wavenumber of ~1600 cm^{-1} (Fig. 7a and b), which corresponds to the bending vibrational mode of water (Kronenberg, 1994) adsorbed on the surface of the gouge. The bending mode is one of the three characteristic molecular vibration modes of water (along with the symmetric and asymmetric stretching modes), where the atomic bond angles are compressed and expanded in an oscillatory manner. The Raman peak associated with the bending vibrational mode was not observed for the starting materials or for samples sheared at low sliding velocities (Fig. S5), only for samples that had been subjected to sliding at seismic slip rates.

We hypothesize that the switch in vibration mode of adsorbed water is caused by a change in chemical bonding on the gouge surface, potentially induced by elevated temperatures during high-velocity shearing, which could be responsible for the rapid healing observed in the SHS experiments (Fig. 4). To investigate this further, we heated undeformed samples of granite and gabbro in an oven to different temperatures (leaving them for ~20 minutes at the target temperature), the samples were then removed from the oven and left to cool at room atmosphere conditions (i.e., the same cooling conditions that the gouge layers experienced during the hold period of the SHS experiments). We analyzed the oven-heated samples using Raman spectroscopy and found the appearance of a small broad peak at ~1600 cm^{-1} for samples that had been heated to temperatures ≥250 °C (Fig. 7c and d), which is similar to the temperatures that the gouge layers experienced during high-velocity shearing where a similar Raman peak was observed (Fig. 7a and

This manuscript is now published at: https://doi.org/10.1029/2023JB026706

b) and also the temperature conditions where rapid healing occurred (Fig. 4). We note that the size of the adsorbed water peak in the oven-heated samples is often less than observed for the sheared gouge samples (particularly for granite), which may be a result the sheared gouges having a much greater surface area due to the presence of nanoparticles (Fig. 6d), producing a stronger Raman signal.

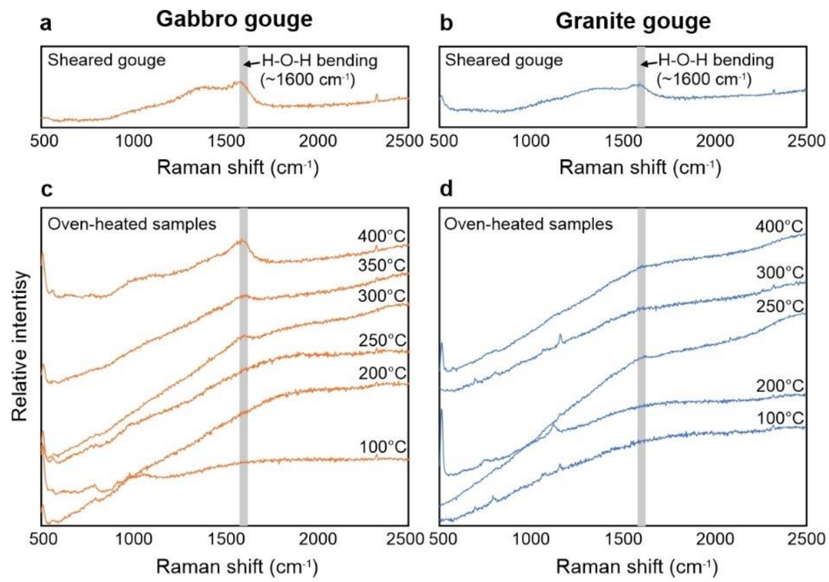

Figure 7: *Raman spectra of the surface of the sheared gabbro* ***(a)*** *and granite (****b****) gouge layers at the end of the high-velocity SHS experiments. Both show a broad peak at a wavenumber of ~1600 cm^{-1}, indicating the bending vibrational mode of H-O-H. Panels (****c****) and (****d****) show Raman spectra for undeformed gabbro and granite samples heated to different temperatures in an oven and then left to cool under atmospheric humidity conditions. The broad peak at 1600 cm^{-1} only appears in samples that have been heated to temperatures ≥250 °C.*

4. Discussion

4.1. Rapid fault healing

The frictional strength data from our high-velocity SHS experiments show that the fault gouges heal rapidly during static hold periods after shearing at seismic slip rates (Fig. 4), in comparison to typical healing rates observed in low-velocity SHS experiments performed at micrometer-per-second slip rates (Carpenter et al., 2016; Dieterich, 1972; Marone, 1997; Marone & Saffer, 2015). The rapid healing rates we observe for the granite and gabbro gouges in our study are a similar order to those observed in previous high-velocity SHS experiments on clay-carbonate-bearing gouges from the Longmenshan fault system (sheared at 0.8 MPa normal stress and a slip rate of 1.4 m/s (Yao et al., 2013)), suggesting that rapid healing after high-velocity slip may be a universal phenomenon that is largely insensitive to the lithology of the fault materials. Rapid healing ($\beta > 0.1$) has also been observed during previous SHS experiments performed at subseismic slip rates (85 mm/s) on bare surfaces (i.e., no gouge, rock-to-rock experiments) of gabbro and granite (Mizoguchi et al., 2006, 2009). We also performed some high-velocity (0.57 m/s) bare-surface SHS experiments using intact samples of granite and gabbro to see whether the healing rates reported by Mizoguchi et al., (2009) would increase at higher slip velocities. However, whereas Mizoguchi et al., (2009) found rapid healing during the static hold periods in their SHS experiments at subseismic slip velocities, we found that during our high-velocity SHS experiments the rock-to-rock samples recovered almost all of their strength during the deceleration phase while the fault was still slipping (Fig. S6), meaning that the healing rate during the static hold period could not be analyzed. Frictional restrengthening during deceleration (similar to coseismic restrengthening in Fig. 1) is commonly observed in high-velocity experiments performed on bare surfaces (Harbord et al., 2021; Proctor et al., 2014; Violay et al., 2019), and implies that the strength recovery mechanisms in operation are able to act so efficiently that the strength increases while the sample is still being sheared. The efficient strength recovery observed during deceleration in previous bare surface experiments may in part be due to the cooling of melt that often forms on the fault surface during high velocity slip (Hirose & Shimamoto, 2005), which can weld the fault together once solidified (Mitchell et al., 2016). However, in our high-velocity bare surface experiments (Fig. S6) no melting was observed on the fault surface, likely due to the relatively low normal stress and slip velocity we used in comparison to previous studies, suggesting that the strength recovery during deceleration is instead caused by frictional healing processes, which potentially operate more efficiently in bare surface experiments due to the highly localized nature of these faults. In contrast, the deformation in gouge experiments is typically distributed across a broader zone (e.g., Fig. 6), which may lead to less efficient strength recovery, resulting in the majority of the healing to occur during the static hold period once slip has ceased (Fig. 4). It should be noted, however, that partial strength recovery during deceleration is sometimes also observed in high-velocity experiments performed on gouge samples, particularly if the deformation is highly localized within the gouge layer (e.g., Sone & Shimamoto, 2009).

Dynamic weakening during the high-velocity shearing events in our experiments (Fig. 3) is likely caused by a combination of flash heating at asperity contacts (Barbery et al., 2021; Harbord et al., 2021; Passelègue et al., 2016; Proctor et al., 2014; Rice, 2006; Sleep, 2019), and the formation of amorphous wear materials (Rowe et al., 2019) and nanoparticles in the gouge (Green et al., 2015; Han et al., 2011; De Paola et al., 2011; Reches & Lockner, 2010). X-ray diffraction analysis of the sheared gouges confirms the presence of amorphous material that was not present in the starting materials (Fig. S7). The microstructures of the sheared gouges (Fig. 6) show no evidence of other weakening mechanisms that have been reported in previous studies such as frictional melting (Hirose & Shimamoto, 2005), silica-gel formation (Goldsby & Tullis, 2002) or grain-size sensitive flow (De Paola et al., 2015; Pozzi et al., 2021). Fault restrengthening during the hold periods is likely caused by the reformation of bonds at asperity contacts in the gouge material. There are two prevailing hypotheses for the time-dependent strengthening of frictional contacts during fault healing: (i) an increase in real contact area by asperity creep (Dieterich & Kilgore, 1994), often referred to as the contact 'quantity' hypothesis, or (ii) the formation of chemical bonds across the asperity interface (Li et al., 2011; Thom et al., 2018), often referred to as the contact 'quality' hypothesis.

If we first consider asperity creep, it is plausible that this process would be more active after seismic slip, as creep is temperature-sensitive and the rapid healing we observe occurs immediately after high-velocity slip while the gouge is still relatively hot (>200 °C, Fig. 4). The likely mechanisms that could facilitate asperity creep are either solution-transfer processes (Rutter, 1983) or indentation creep (Scholz & Engelder, 1976). Solution-transfer is unlikely to be a dominant mechanism in our experiments as they were run without a pore-fluid (i.e., room atmosphere conditions), therefore there is no solute to transfer chemical species. Furthermore, previous fault healing experiments under hydrothermal conditions, where solution-transfer processes are operative, show complex non-log-linear healing behavior (van den Ende & Niemeijer, 2019; Jeppson & Lockner, 2022; Karner et al., 1997; Nakatani & Scholz, 2004) that is quite different to the healing trends we observe in our data (Fig. 4). Indentation creep can operate under atmospheric conditions in the absence of a pore-fluid (Frye & Marone, 2002), however, although previous low-velocity fault healing experiments at elevated temperatures (up to 550°C) under room humidity conditions indicate some temperature-dependence on healing rate (Mitchell et al., 2013; Nakatani, 2001), the effect is relatively minor (for intact granite Mitchell et al., (2013) found that β increases from 0.016 at room temperature to 0.021 at 500°C) and insufficient to explain the rapid healing in our experiments. Additionally, if asperity creep were responsible for the rapid healing it would be expected that the gouge would also exhibit a linear log-time compaction relationship during the hold period (Sleep, 2006), which we do not observe in our mechanical data (Fig. 5e and f); the log-time compaction relationship in our experiments is particularly non-linear during the initial stages of the hold period when the rapid healing occurs ($t_h < 20$ s). This observation potentially supports the suggestion from recent granular fault gouge simulation studies that fault healing can be decoupled from changes in gouge layer thickness due to compaction/dilation (Ferdowsi & Rubin, 2020, 2021). Based on the rationale outlined above we believe that, although asperity creep may be operating during the static hold period, it is unlikely that an increase in the real contact area is the dominant cause of the rapid restrengthening we observe in our high-velocity SHS experiments. However, we note that asperity creep may become a more dominant healing mechanism during the second, slower healing phase that we observe (Fig. 4), when β is comparable to healing rates observed in low-velocity SHS experiments.

An alternative explanation for rapid healing is that it may be caused by enhanced chemical bonding across contacting asperity interfaces. Our Raman data reveal a change in chemical bonding on the surface of the gouges sheared at high-velocity, with a switch in the vibrational mode of adsorbed water to the H-O-H bending mode, which only occurs after the sample has been heated to temperatures ≥250 °C (Fig. 7c-d). Although we observe a change in adsorbed water properties, we do not expect the adsorbed water itself to be responsible for the rapid healing, as rapid healing occurs at temperatures >200 °C (Fig. 4) where water would be in the vapor state and desorbed from the gouge surface (Reches & Lockner, 2010). Instead, we hypothesize that the rapid healing is a result of hydrogen bonding on the surface of the sheared gouge materials, which subsequently causes water to re-adsorb in the bending vibrational mode once the gouge has cooled to sufficiently low temperatures (<140 °C) (Reches & Lockner, 2010) during the hold period. Hydrogen bonding can arise between hydroxylated silanol (Si-OH) surfaces (Michalske & Fuller, 1985), which are readily formed on freshly cleaved surfaces of silicate materials during frictional slip (Hirose et al., 2011; Kronenberg, 1994; Rowe et al., 2019) (Fig. 8a). Once slip has stopped, the formation of hydrogen bonds between silanol surfaces can take place on very short timescales ($<10^{-2}$ s) (Liu & Szlufarska, 2012). Therefore, if hydrogen bonding occurs during the first few seconds of static hold in our experiments, it could be responsible for the rapid increase in friction we observe. Furthermore, at elevated temperatures, like those produced by shear heating in our experiments, silanol groups on opposite sides of an asperity interface can react to form strong covalent siloxane (Si-O-Si) bonds (Shioji et al., 2001; Vigil et al., 1994) (Fig. 8b). Previous molecular dynamics simulations of silica-silica interfaces have shown that siloxane bond formation provides a plausible explanation for frictional healing, with frictional strength being approximately proportional to the number of siloxane bonds (Li et al., 2014) and the kinetics of interfacial bond formation leading to a logarithmic time-dependent increase in strength (Liu & Szlufarska, 2012), as observed in SHS experiments (Fig. 4). Therefore, we postulate that rapid healing after high-velocity slip is caused by either hydrogen or siloxane bond formation (or a combination of both) at asperity contacts in the sheared gouges. Once the gouge has cooled to sufficiently low temperature water will re-adsorb (Reches & Lockner, 2010) (Fig. 8c). The vibrational motions of water molecules are sensitive to local hydrogen bonding on the adsorbent surface (Kronenberg, 1994; Shioji et al., 2001), thus the switch to the H-O-H bending mode we observe on the sheared gouges likely results from changes in the hydrogen bonding on the gouge surface that occur during/after high-velocity slip while the gouge is still hot, hence why the change in adsorbed water properties is only observed in samples that have been heated to temperatures >250 °C (Fig. 7c-d) and not in the samples sheared at low velocity where the temperature increase was low.

The hypothesis that rapid healing is caused by enhanced hydrogen bonding is also supported by the experimental results of Mizoguchi et al., (2006), who find that rapid healing is suppressed in their bare surface SHS experiments on intact gabbro samples (sheared at 85 mm/s) when they are performed in a nitrogen atmosphere, instead of at room humidity conditions. Although Mizoguchi et al., (2006, 2009) interpret this to mean that rapid healing is caused by water adsorption onto the fault surface during the static hold period (they calculate a maximum temperature due to shear heating of ~100 °C in their subseismic SHS experiments), we have shown that water adsorption cannot be responsible, as the rapid healing in our high-velocity experiments occurs early during the static hold period (Fig. 4) while the sample temperature is too high for water adsorption (>200 °C). Instead, we postulate that the suppressed healing in the nitrogen experiments of Mizoguchi et al., (2006) is due to a lack of hydrogen bonding in this environment. When there is no moisture available, hydroxylated silanol (SiOH) will be unable to form on the surface of the fault materials during shearing, which will in turn limit any hydrogen bonding across asperity interfaces during the static hold period. The results of Mizoguchi et al., (2006, 2009) are therefore consistent with our hypothesis that rapid healing is caused by enhanced chemical bond formation across asperity interfaces.

This manuscript is now published at: https://doi.org/10.1029/2023JB026706

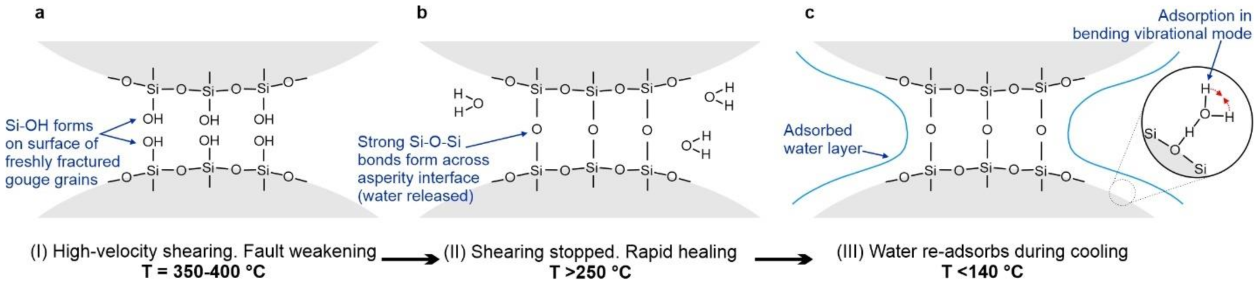

Figure 8: *Schematic cartoon showing the evolution of chemical bonding during and after high-velocity slip. (**a**) Silanol bonds (Si-OH) form on freshly fractured gouge surfaces during high-velocity slip. During the hold period, once fault slip has ceased, we hypothesize that rapid healing occurs as a result of either hydrogen bonding between adjacent silanol surfaces, or (**b**) the formation of strong siloxane bonds across the asperity interface. (**c**) Once the gouge has cooled to temperatures <140 °C during the hold period, water re-adsorbs onto the surface in the bending vibrational mode.*

4.2. Implications for fault strength evolution and earthquake recurrence

Regardless of the underlying restrengthening mechanism, our data clearly show that fault materials heal rapidly after seismic slip, which has important implications for our understanding of the earthquake cycle. Rapid healing may explain why geophysical observations suggest some faults regain their strength early during interseismic periods after large earthquakes (Magen et al., 2020; Tadokoro & Ando, 2002; Xue et al., 2013). Fast-acting healing mechanisms, like those in operation during our experiments, potentially also operate during coseismic slip on natural faults, particularly when slip occurs heterogeneously along the fault such as during the propagation of pulse-like ruptures (Galetzka et al., 2015; Heaton, 1990; Lambert et al., 2021; Wang & Barbot, 2023). The passage of a rupture pulse requires rapid healing in the just-slipped portions of the fault (Perrin et al., 1995), in order for them to stay locked and prevent further slip as they are reloaded by waves from the actively slipping regions elsewhere along the fault. It is plausible that the rapid healing mechanisms in our experiments become faster acting at the pressure-temperature conditions associated with seismogenic depths in nature, meaning that they could potentially contribute to the generation of pulse-like ruptures. Results from recent dynamic rupture experiments further highlight the complex interplay between rapid weakening and healing processes that occur in gouge samples during dynamic rupture propagation (Rubino et al., 2022). Future studies at higher normal stress and ambient temperatures, as well as in the presence of pore fluids, are required to investigate how the rates of frictional healing evolve with depth in the Earth's crust. We note that our experiments were run under nominally dry conditions, whereas crustal faults will typically be fluid saturated. The presence of fluids may buffer the coseismic temperature rise and dissipate heat away from the grain contacts more efficiently than in our experiments, potentially slowing any thermally activated healing mechanisms in operation; as well as producing fluid pressure transients via thermal pressurization (Badt et al., 2020; Rice, 2006) that may maintain fault weakness in the initial stages of the postseismic regime if fluids are unable to dissipate efficiently. However, most crustal faults will be active under greater normal stresses than imposed on the gouge samples in our experiments, which will lead to greater amounts of shear heating, potentially enhancing the rates of postseismic fault healing. More experiments and theoretical studies are therefore required to test how fault healing operates under the range of possible conditions that faults experience at seismogenic depths in nature, where there is a competition between heat generation and dissipation processes.

Rapid fault strength recovery immediately following a seismic event suggests that earthquake recurrence is not necessarily controlled by continuous restrengthening over time during interseismic periods. Instead, if the majority of strength is recovered early during the interseismic period, as implied by our results, then earthquake recurrence on natural faults may be more strongly controlled by far-field tectonic loading (i.e., when the buildup of stress applied to the fault exceeds the strength an earthquake may occur). Alternatively, other time-dependent processes in operation during interseismic periods may influence earthquake recurrence. For example, over typical recurrence intervals of hundreds of years, fault cohesion will also increase by longer timescale processes such a cementation and pressure solution (van den Ende & Niemeijer, 2019; Muhuri et al., 2003; Tenthorey & Cox, 2006). The resulting increase in cohesion and lithification of the fault gouge will not only contribute to the fault strength evolution, but will also influence the frictional stability of the gouge materials, with more cohesive materials often displaying rate-weakening behavior required for earthquake nucleation (Ikari & Hüpers, 2021; Roesner et al., 2020). It is plausible that transitions from rate-strengthening to rate-weakening behavior may occur as the gouge materials become more lithified during interseismic periods, potentially leading to earthquake recurrence once the frictional properties have evolved to a state that promotes earthquake nucleation and unstable slip.

5. Conclusions

In summary, we find that faults regain their strength rapidly after experiencing dynamic weakening during seismic slip. After the initial rapid increase in strength back to pre-seismic strength levels, the healing rate decreases to a rate that is comparable to those observed in low-velocity friction experiments. Rapid healing occurs while the gouge is still relatively hot from shear heating, and is likely promoted by enhanced chemical bonding across contacting asperity interfaces. Further experimental and theoretical studies are needed to investigate the kinetics of interfacial reactions over the range of stress, temperature and pore fluid conditions that faults experience during and after earthquake slip, to understand better strength recovery at seismogenic depths. Our findings motivate further study aimed at the quantification of rapid healing mechanisms and incorporation into larger-scale constitutive laws for modelling dynamic fault processes, to provide insight into the driving mechanisms of earthquake rupture and arrest, and hence seismic hazard.

Acknowledgments

We are grateful to Takahiro Suzuki and Osamu Tadai for technical support with the experiments and analyses. We thank Marco Scuderi and an anonymous reviewer whose comments significantly improved the manuscript, we also thank Kyuichi Kanagawa for comments on an earlier version of the manuscript. This work was supported by a Japan Society for the Promotion of Science (JSPS) International Research

This manuscript is now published at: https://doi.org/10.1029/2023JB026706

Fellowship and JSPS KAKENHI Grant Numbers JP20F20786 and JP19K21907. The associated experimental data files for this research can be accessed at: https://data.mendeley.com/datasets/rw3ndtwkgt/1

References

Badt, N. Z., Tullis, T. E., Hirth, G., & Goldsby, D. L. (2020). Thermal pressurization weakening in laboratory experiments. *Journal of Geophysical Research: Solid Earth*, *125*, e2019JB018872. https://doi.org/10.1029/2019JB018872

Barbery, M. R., Chester, F. M., & Chester, J. S. (2021). Characterizing the distribution of temperature and normal stress on flash heated granite surfaces at seismic slip rates. *Journal of Geophysical Research: Solid Earth*, *126*, e2020JB021353. https://doi.org/10.1029/2020JB021353

Baumberger, T., & Caroli, C. (2006). Solid friction from stick–slip down to pinning and aging. *Advances in Physics*, *55*(3–4), 279–348. https://doi.org/10.1080/00018730600732186

Bedford, J. D., & Faulkner, D. R. (2021). The role of grain size and effective normal stress on localization and the frictional stability of simulated quartz gouge. *Geophysical Research Letters*, *48*(7), e2020GL092023. https://doi.org/10.1029/2020gl092023

Beeler, N. M., Tullis, T. E., & Weeks, J. D. (1994). The roles of time and displacement in the evolution effect in rock friction. *Geophysical Research Letters*, *21*(18), 1987–1990. https://doi.org/10.1029/94GL01599

Boulton, C., Yao, L., Faulkner, D. R., Townend, J., Toy, V. G., Sutherland, R., et al. (2017). High-velocity frictional properties of Alpine Fault rocks: Mechanical data, microstructural analysis, and implications for rupture propagation. *Journal of Structural Geology*, *97*, 71–92. https://doi.org/10.1016/j.jsg.2017.02.003

This manuscript is now published at: https://doi.org/10.1029/2023JB026706

Carpenter, B. M., Ikari, M. J., & Marone, C. (2016). Laboratory observations of time-dependent frictional strengthening and stress relaxation in natural and synthetic fault gouges. *Journal of Geophysical Research: Solid Earth*, *121*, 1183–1201. https://doi.org/10.1002/2015JB012136

De Paola, N., Hirose, T., Mitchell, T., Di Toro, G., Viti, C., & Shimamoto, T. (2011). Fault lubrication and earthquake propagation in thermally unstable rocks. *Geology*, *39*(1), 35–38. https://doi.org/10.1130/G31398.1

De Paola, N., Holdsworth, R. E., Viti, C., Collettini, C., & Bullock, R. (2015). Can grain size sensitive flow lubricate faults during the initial stages of earthquake propagation? *Earth and Planetary Science Letters*, *431*, 48–58. https://doi.org/10.1016/j.epsl.2015.09.002

Dieterich, J. H. (1972). Time-dependent friction in rocks. *Journal of Geophysical Research*, *77*(20), 3690–3697. https://doi.org/10.1029/JB077i020p03690

Dieterich, J. H., & Kilgore, B. D. (1994). Direct observation of frictional contacts: New insights for state-dependent properties. *Pure and Applied Geophysics*, *143*, 283–302. https://doi.org/10.1007/BF00874332

Di Toro, G., Han, R., Hirose, T., De Paola, N., Nielsen, S., Mizoguchi, K., et al. (2011). Fault lubrication during earthquakes. *Nature*, *471*, 494–498. https://doi.org/10.1038/nature09838

Ferdowsi, B., & Rubin, A. M. (2020). A granular physics-based view of fault friction experiments. *Journal of Geophysical Research: Solid Earth*, *125*, e2019JB019016. https://doi.org/10.1029/2019JB019016

Ferdowsi, B., & Rubin, A. M. (2021). Slide-hold-slide protocols and frictional healing in discrete element method (DEM) simulations of granular fault gouge. *Journal of Geophysical Research: Solid Earth*, *126*, e2021JB022125. https://doi.org/10.1029/2021JB022125

Frye, K. M., & Marone, C. (2002). Effect of humidity on granular friction at room temperature. *Journal of Geophysical Research*, *107*(B11), 2309. https://doi.org/10.1029/2001jb000654

Galetzka, J., Melgar, D., Genrich, J. F., Geng, J., Owen, S., Lindsey, E. O., et al. (2015). Slip pulse and resonance of the Kathmandu basin during the 2015 Gorkha earthquake, Nepal. *Science*, *349*(6252), 1091–1096. https://doi.org/10.1126/science.aac6383

Giacomel, P., Ruggieri, R., Scuderi, M. M., Spagnuolo, E., Di Toro, G., & Collettini, C. (2021). Frictional properties of basalt experimental faults and implications for volcano-tectonic settings and geo-energy sites. *Tectonophysics*, *811*, 228883. https://doi.org/10.1016/j.tecto.2021.228883

Goldsby, D. L., & Tullis, T. E. (2002). Low frictional strength of quartz rocks at subseismic slip rates. *Geophysical Research Letters*, *29*(17), 1844. https://doi.org/10.1029/2002GL015240

Green, H. W., Shi, F., Bozhilov, K., Xia, G., & Reches, Z. (2015). Phase transformation and nanometric flow cause extreme weakening during fault slip. *Nature Geoscience*, *8*, 484–489. https://doi.org/10.1038/NGEO2436

Han, R., Shimamoto, T., Hirose, T., Ree, J. H., & Ando, J. (2007). Ultralow friction of carbonate faults caused by thermal decomposition. *Science*, *316*(5826), 878–881. https://doi.org/10.1126/science.1139763

Han, R., Hirose, T., Shimamoto, T., Lee, Y., & Ando, J. (2011). Granular nanoparticles lubricate faults during seismic slip. *Geology*, *39*(6), 599–602. https://doi.org/10.1130/G31842.1

Harbord, C., Brantut, N., Spagnuolo, E., & Di Toro, G. (2021). Fault friction during simulated seismic slip pulses. *Journal of Geophysical Research: Solid Earth*, *126*, e2021JB022149. https://doi.org/10.1029/2021JB022149

Heaton, T. H. (1990). Evidence for and implications of self-healing pulses of slip in earthquake rupture. *Physics of the Earth and Planetary Interiors*, *64*, 1–20. https://doi.org/10.1016/0031-9201(90)90002-F

Hirose, T., & Shimamoto, T. (2005). Growth of molten zone as a mechanism of slip weakening of simulated faults in gabbro during frictional melting. *Journal of Geophysical Research*, *110*, B05202.

https://doi.org/10.1029/2004JB003207

Hirose, T., Kawagucci, S., & Suzuki, K. (2011). Mechanoradical H_2 generation during simulated faulting: Implications for an earthquake-driven subsurface biosphere. *Geophysical Research Letters*, *38*, L17303. https://doi.org/10.1029/2011GL048850

Hunfeld, L. B., Chen, J., Niemeijer, A. R., Ma, S., & Spiers, C. J. (2021). Seismic slip-pulse experiments simulate induced earthquake rupture in the Groningen gas field. *Geophysical Research Letters*, *48*, e2021GL092417. https://doi.org/10.1029/2021GL092417

Ikari, M. J., & Hüpers, A. (2021). Velocity-weakening friction induced by laboratory-controlled lithification. *Earth and Planetary Science Letters*, *554*, 116682. https://doi.org/10.1016/j.epsl.2020.116682

Jeppson, T., & Lockner, D. (2022). Impact of fluid-rock interaction on strength and hydraulic transmissivity evolution in shear fractures under hydrothermal conditions. In *47th Workshop on Geothermal Reservoir Engineering*. Stanford, California.

Kanamori, H., & Allen, C. R. (1986). Earthquake repeat time and average stress drop. In S. Das, J. Boatwright, & C. H. Scholz (Eds.), *Earthquake Source Mechanics* (Vol. 37, pp. 227–235). Washington D.C.: American Geophysical Union. https://doi.org/10.1029/GM037p0227

Kaneki, S., Oohashi, K., Hirono, T., & Noda, H. (2020). Mechanical amorphization of synthetic fault gouges during rotary-shear friction experiments at subseismic to seismic slip velocities. *Journal of Geophysical Research: Solid Earth*, *125*, e2020JB019956. https://doi.org/10.1029/2020JB019956

Karner, S. L., Marone, C., & Evans, B. (1997). Laboratory study of fault healing and lithification in simulated fault gouge under hydrothermal conditions. *Tectonophysics*, *277*, 41–55. https://doi.org/10.1016/S0040-1951(97)00077-2

Kronenberg, A. K. (1994). Hydrogen speciation and chemical weakening of quartz. In P. J. Heaney, C. T. Prewitt, & G. V Gibbs (Eds.), *Silica: Physical Behaviour, Geochemistry and Materials Applications* (pp. 123–176). Mineralogical Society of America.

Lambert, V., Lapusta, N., & Perry, S. (2021). Propagation of large earthquakes as self-healing pulses or mild cracks. *Nature*, *591*, 252–258. https://doi.org/10.1038/s41586-021-03248-1

Li, A., Liu, Y., & Szlufarska, I. (2014). Effects of interfacial bonding on friction and wear at silica/silica interfaces. *Tribology Letters*, *56*, 481–490. https://doi.org/10.1007/s11249-014-0425-x

Li, Q., Tullis, T. E., Goldsby, D., & Carpick, R. W. (2011). Frictional ageing from interfacial bonding and the origins of rate and state friction. *Nature*, *480*, 233–236. https://doi.org/10.1038/nature10589

Li, Y.-G., Chen, P., Cochran, E. S., Vidale, J. E., & Burdette, T. (2006). Seismic evidence for rock damage and healing on the San Andreas Fault associated with the 2004 M 6.0 Parkfield earthquake. *Bulletin of the Seismological Society of America*, *96*(4B), S349–S363. https://doi.org/10.1785/0120050803

Liu, Y., & Szlufarska, I. (2012). Chemical origins of frictional aging. *Physical Review Letters*, *109*(186102). https://doi.org/10.1103/PhysRevLett.109.186102

Magen, Y., Ziv, A., Inbal, A., Baer, G., & Hollingsworth, J. (2020). Fault rerupture during the July 2019 Ridgecrest earthquake pair from joint slip inversion of InSAR, optical imagery, and GPS. *Bulletin of the Seismological Society of America*, *110*, 1627–1643. https://doi.org/10.1785/0120200024

Marone, C. (1997). On the rate of frictional healing and the constitutive law for time- and slip-dependent friction. *International Journal of Rock Mechanics & Mining Sciences*, *34*(3–4), 187.e1-187.e17. https://doi.org/10.1016/S1365-1609(97)00054-3

Marone, C. (1998). The effect of loading rate on static friction and the rate of fault healing during the earthquake cycle. *Nature*, *391*, 69–72. https://doi.org/10.1038/34157

Marone, C., & Saffer, D. M. (2015). The mechanics of frictional healing and slip instability during the seismic cycle. In G. Schubert (Ed.), *Treatise on Geophysics* (2nd ed., Vol. 4, pp. 111–138). Elsevier.

https://doi.org/10.1016/B978-0-444-53802-4.00092-0

Marone, C., Vidale, J. E., & Ellsworth, W. L. (1995). Fault healing inferred from time dependent variations in source properties of repeating earthquakes. *Geophysical Research Letters*, *22*(22), 3095–3098. https://doi.org/10.1029/95GL03076

McLaskey, G. C., Thomas, A. M., Glaser, S. D., & Nadeau, R. M. (2012). Fault healing promotes high-frequency earthquakes in laboratory experiments and on natural faults. *Nature*, *491*, 101–104. https://doi.org/10.1038/nature11512

Michalske, T. A., & Fuller, E. R. (1985). Closure and repropagation of healed cracks in silicate glass. *Journal of the American Ceramic Society*, *68*(11), 586–590. https://doi.org/10.1111/j.1151-2916.1985.tb16160.x

Mitchell, E. K., Fialko, Y., & Brown, K. M. (2013). Temperature dependence of frictional healing of Westerly granite: Experimental observations and numerical simulations. *Geochemistry, Geophysics, Geosystems*, *14*(3), 567–582. https://doi.org/10.1029/2012GC004241

Mitchell, T. M., Toy, V., Di Toro, G., Renner, J., & Sibson, R. H. (2016). Fault welding by pseudotachylyte formation. *Geology*, *44*(12), 1059–1062. https://doi.org/10.1130/G38373.1

Mizoguchi, K., Hirose, T., Shimamoto, T., & Fukuyama, E. (2006). Moisture-related weakening and strengthening of a fault activated at seismic slip rates. *Geophysical Research Letters*, *33*, L16319. https://doi.org/10.1029/2006GL026980

Mizoguchi, K., Hirose, T., Shimamoto, T., & Fukuyama, E. (2009). Fault heals rapidly after dynamic weakening. *Bulletin of the Seismological Society of America*, *99*(6), 3470–3474. https://doi.org/10.1785/0120080325

Muhuri, S. K., Dewers, T. A., Scott Jr., T. E., & Reches, Z. (2003). Interseismic fault strengthening and earthquake-slip instability: Friction or cohesion? *Geology*, *31*(10), 881–884. https://doi.org/10.1130/G19601.1

Nakatani, M. (2001). Conceptual and physical clarification of rate and state friction: Frictional sliding as a thermally activated rheology. *Journal of Geophysical Research*, *106*(B7), 13347–13380. https://doi.org/10.1029/2000JB900453

Nakatani, M., & Scholz, C. H. (2004). Frictional healing of quartz gouge under hydrothermal conditions: 1. Experimental evidence for solution transfer healing mechanism. *Journal of Geophysical Research*, *109*, B07201. https://doi.org/10.1029/2001JB001522

Orellana, L. F., Scuderi, M. M., Collettini, C., & Violay, M. (2018). Do scaly clays control seismicity on faulted shale rocks? *Earth and Planetary Science Letters*, *488*, 59–67. https://doi.org/10.1016/j.epsl.2018.01.027

Park, Y., Hirose, T., & Ree, J.-H. (2021). Carbonate fault mirrors with extremely low frictional healing rates: A possible source of aseismic creep. *Geophysical Research Letters*, *48*, e2021GL093749. https://doi.org/10.1029/2021GL093749

Passelègue, F. X., Spagnuolo, E., Violay, M., Nielsen, S., Di Toro, G., & Schubnel, A. (2016). Frictional evolution, acoustic emissions activity, and off-fault damage in simulated faults sheared at seismic slip rates. *Journal of Geophysical Research: Solid Earth*, *121*(10), 7490–7513. https://doi.org/10.1002/2016JB012988

Pei, S., Niu, F., Ben-Zion, Y., Sun, Q., Liu, Y., Xue, X., et al. (2019). Seismic velocity reduction and accelerated recovery due to earthquakes on the Longmenshan fault. *Nature Geoscience*, *12*, 387–392. https://doi.org/10.1038/s41561-019-0347-1

Perrin, G., Rice, J. R., & Zheng, G. (1995). Self-healing slip pulse on a frictional surface. *Journal of the Mechanics and Physics of Solids*, *43*(9), 1461–1495. https://doi.org/10.1016/0022-5096(95)00036-I

Pozzi, G., De Paola, N., Nielsen, S. B., Holdsworth, R. E., Tesei, T., Thieme, M., & Demouchy, S. (2021). Coseismic fault lubrication by viscous deformation. *Nature Geoscience*, *14*, 437–442. https://doi.org/10.1038/s41561-021-00747-8

Proctor, B. P., Mitchell, T. M., Hirth, G., Goldsby, D., Zorzi, F., Platt, J. D., & Di Toro, G. (2014). Dynamic weakening of serpentinite gouges and bare surfaces at seismic slip rates. *Journal of Geophysical Research: Solid Earth*, *119*, 8107–8131. https://doi.org/10.1002/2014JB011057

Reches, Z., & Lockner, D. A. (2010). Fault weakening and earthquake instability by powder lubrication. *Nature*, *467*, 452–455. https://doi.org/10.1038/nature09348

Rempe, M., Di Toro, G., Mitchell, T. M., Smith, S. A. F., Hirose, T., & Renner, J. (2020). Influence of effective stress and pore fluid pressure on fault strength and slip localization in carbonate slip zones. *Journal of Geophysical Research: Solid Earth*, *125*, e2020JB019805. https://doi.org/10.1029/2020JB019805

Rice, J. R. (2006). Heating and weakening of faults during earthquake slip. *Journal of Geophysical Research*, *111*(B05311). https://doi.org/10.1029/2005JB004006

Roesner, A., Ikari, M. J., Saffer, D. M., Stanislowski, K., Eijsink, A. M., & Kopf, A. J. (2020). Friction experiments under in-situ stress reveal unexpected velocity-weakening in Nankai accretionary prism samples. *Earth and Planetary Science Letters*, *538*(116180). https://doi.org/10.1016/j.epsl.2020.116180

Rowe, C. D., Lamothe, K., Rempe, M., Andrews, M., Mitchell, T. M., Di Toro, G., et al. (2019). Earthquake lubrication and healing explained by amorphous nanosilica. *Nature Communications*, *10*(1), 1–11. https://doi.org/10.1038/s41467-018-08238-y

Rubino, V., Lapusta, N., & Rosakis, A. J. (2022). Intermittent lab earthquakes in dynamically weakening fault gouge. *Nature*, *606*, 922–929. https://doi.org/10.1038/s41586-022-04749-3

Rutter, E. H. (1983). Pressure solution in nature, theory and experiment. *Journal of the Geological Society*, *140*(5), 725–740. https://doi.org/10.1144/gsjgs.140.5.0725

Sammis, C. G., & Ben-Zion, Y. (2008). Mechanics of grain-size reduction in fault zones. *Journal of Geophysical Research: Solid Earth*, *113*(B02306). https://doi.org/10.1029/2006JB004892

Scholz, C. H., & Engelder, J. T. (1976). The role of asperity indentation and ploughing in rock friction - I. Asperity creep and stick-slip. *International Journal of Rock Mechanics and Mining Sciences and Geomechanical Abstracts*, *13*(5), 149–154. https://doi.org/10.1016/0148-9062(76)90819-6

Scholz, C. H., Aviles, C. A., & Wesnousky, S. G. (1986). Scaling differences between large interplate and intraplate earthquakes. *Bulletin of the Seismological Society of America*, *76*(1), 65–70. https://doi.org/10.1785/BSSA0760010065

Scuderi, M. M., & Carpenter, B. M. (2022). Frictional stability and hydromechanical coupling of serpentinite-bearing fault gouge. *Geophysical Journal International*, *231*, 290–305. https://doi.org/10.1093/gji/ggac188

Seyler, C. E., Kirkpatrick, J. D., Savage, H. M., Hirose, T., & Faulkner, D. R. (2020). Rupture to the trench? Frictional properties and fracture energy of incoming sediments at the Cascadia subduction zone. *Earth and Planetary Science Letters*, *546*, 116413. https://doi.org/10.1016/j.epsl.2020.116413

Shioji, S., Kawaguchi, M., Hayashi, Y., Tokami, K., & Yamamoto, H. (2001). Rehydroxylation of dehydrated silica surfaces by water vapor adsorption. *Advanced Powder Technology*, *12*(3), 331–342. https://doi.org/10.1163/156855201750537884

Shreedharan, S., Saffer, D., Wallace, L. M., & Williams, C. (2023). Ultralow frictional healing explains recurring slow slip events. *Science*, *379*(6633), 712–717. https://doi.org/10.1126/science.adf4930

Sleep, N. H. (2006). Real contacts and evolution laws for rate and state friction. *Geochemistry Geophysics Geosystems*, *7*(8), Q08012. https://doi.org/10.1029/2005GC001187

Sleep, N. H. (2019). Thermal weakening of asperity tips on fault planes at high sliding velocities. *Geochemistry, Geophysics, Geosystems*, *20*, 1164–1188. https://doi.org/10.1029/2018GC008062

Sone, H., & Shimamoto, T. (2009). Frictional resistance of faults during accelerating and decelerating earthquake slip. *Nature Geoscience*, *2*, 705–708. https://doi.org/10.1038/ngeo637

This manuscript is now published at: https://doi.org/10.1029/2023JB026706

Tadokoro, K., & Ando, M. (2002). Evidence for rapid fault healing derived from temporal changes in S wave splitting. *Geophysical Research Letters*, *29*(4), 1047. https://doi.org/10.1029/2001GL013644

Tanikawa, W., Mukoyoshi, H., & Tadai, O. (2012). Experimental investigation of the influence of slip velocity and temperature on permeability during and after high-velocity fault slip. *Journal of Structural Geology*, *38*, 90–101. https://doi.org/10.1016/j.jsg.2011.08.013

Tenthorey, E., & Cox, S. F. (2006). Cohesive strengthening of fault zones during the interseismic period: An experimental study. *Journal of Geophysical Research*, *111*(B09202). https://doi.org/10.1029/2005JB004122

Thom, C. A., Carpick, R. W., & Goldsby, D. L. (2018). Constraints on the physical mechanism of frictional aging from nanoindentation. *Geophysical Research Letters*, *45*, 13306–13311. https://doi.org/10.1029/2018GL080561

Tsutsumi, A., & Shimamoto, T. (1997). High-velocity frictional properties of gabbro. *Geophysical Research Letters*, *24*(6), 699–702. https://doi.org/10.1029/97GL00503

Tullis, T. E. (2015). Mechanisms for friction of rock at earthquake slip rates. In G. Schubert (Ed.), *Treatise on Geophysics* (2nd ed., Vol. 4, pp. 139–159). Elsevier. https://doi.org/10.1016/B978-0-444-53802-4.00073-7

van den Ende, M. P. A., & Niemeijer, A. R. (2019). An investigation into the role of time-dependent cohesion in interseismic fault restrengthening. *Scientific Reports*, *9*, 9894. https://doi.org/10.1038/s41598-019-46241-5

Vidale, J. E., Ellsworth, W. L., Cole, A., & Marone, C. (1994). Variations in rupture process with recurrence interval in a repeated small earthquake. *Nature*, *368*, 624–626. https://doi.org/10.1038/368624a0

Vigil, G., Xu, Z., Steinberg, S., & Israelachvili, J. (1994). Interactions of silica surfaces. *Journal of Colloid and Interface Science*, *165*, 367–385. https://doi.org/10.1006/jcis.1994.1242

Violay, M., Passelegue, F., Spagnuolo, E., Di Toro, G., & Cornelio, C. (2019). Effect of water and rock composition on re-strengthening of cohesive faults during the deceleration phase of seismic slip pulses. *Earth and Planetary Science Letters*, *522*, 55–64. https://doi.org/10.1016/j.epsl.2019.06.027

Wang, B., & Barbot, S. (2023). Pulse-like ruptures, seismic swarms, and tremorgenic slow-slip events with thermally activated friction. *Earth and Planetary Science Letters*, *603*, 117983. https://doi.org/10.1016/j.epsl.2022.117983

Xue, L., Li, H.-B., Brodsky, E. E., Xu, Z.-Q., Kano, Y., Wang, H., et al. (2013). Continuous permeability measurements record healing inside the Wenchuan earthquake fault zone. *Science*, *340*(6140), 1555–1559. https://doi.org/10.1126/science.1237237

Yao, L., Shimamoto, T., Ma, S., Han, R., & Mizoguchi, K. (2013). Rapid postseismic strength recovery of Pingxi fault gouge from the Longmenshan fault system: Experiments and implications for the mechanisms of high-velocity weakening of faults. *Journal of Geophysical Research: Solid Earth*, *118*, 4547–4563. https://doi.org/10.1002/jgrb.50308